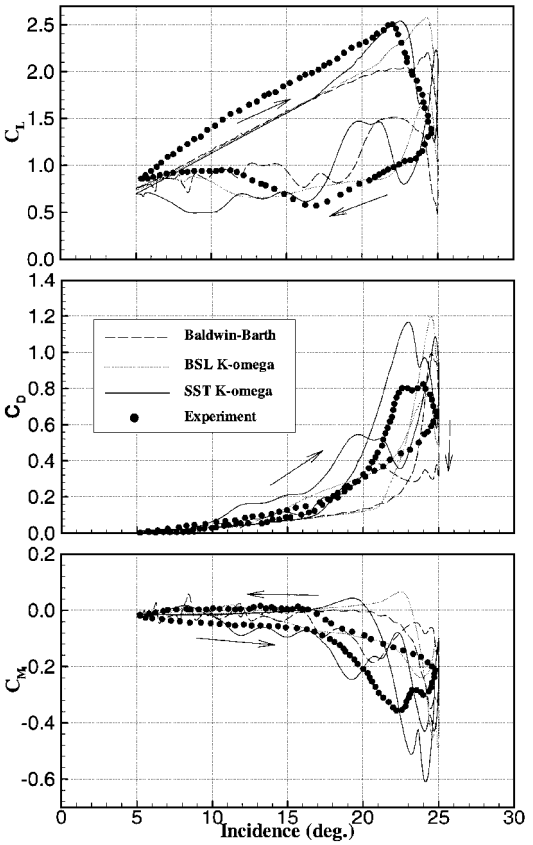

Fig. 3 Hysteresis loops, VR-7.

Its computed maximum value is overestimated with all models. This experimental value is extremely inferior to those found for the preceding case. The negative damping of the computed moment coefficient found with all of the turbulence models does not exist in the experimental data. None of the models give results that correspond to experimental data. The minimum experimental moment coefficient is -0.37 as for the Sikorsky SC-1095; this value is -0.49, and for the NACA 0012 it is -0.45. Therefore, this is the weaker minimum.

Instantaneous streamline pictures are used only for qualitative comparison of different turbulence models. For all airfoil shapes used, with the SST $K-\omega$ model turbulence model, the leading edge vortex spreads over the upper surface. With a NACA 0012 airfoil or a VR-7 airfoil, a trailing-edge vortex exists and the leading-edge vortex begins to shed. The BSL $K-\omega$ model predicts a trailing-edge eddy on the SC-1095 and VR-7 airfoils.

The flow difference between both airfoil shapes is the leading-edge vortex structure. On the SC-1095 airfoil, it is composed of a double structure. A trailing-edge eddy is predicted with the B–B turbulence model. On the SC-1095 airfoil, it is shed. The leading-edge vortex is composed of the same structure on the NACA 0012 and VR-7 airfoils.

Conclusions

The unsteady two-dimensional flowfield of an oscillating airfoil is calculated with the intention of evaluating the ability of one- and two-equation turbulence models to predict the unsteady separated flows of dynamic stall. Several airfoil shapes are used. For all test cases, the lift hysteresis, predicted by all turbulence models, is underestimated during the upstroke. The B–B model performs poorly in predicting pitching moment for all airfoil shapes. A difference exists between results given by the BSL and SST $K-\omega$ turbulence models, but neither model can be qualified as better than the other.

Acknowledgments

The authors gratefully acknowledge the Scientific Committee of the Institut du Développement et des Ressources en Informatique Scientifique du Centre National de la Recherche Scientifique (IDRIS) (Projects 96.0129 and 97.0129) for the use of CPU time on the IDRIS Cray 98.

References

[1]McCroskey, W. J., "The Phenomenon of Dynamic Stall," NASA TM-81264, March 1981.

[2]Carr, L. W., "Progress in Analysis and Prediction of Dynamic Stall," *Journal of Aircraft*, Vol. 25, No. 1, 1988, pp. 6–17.

[3]Deng, G. B., Guilmineau, E., Piquet, J., Queutey, P., and Visonneau, M., "Computation of Unsteady Laminar Viscous Flow Past an Aerofoil," *International Journal for Numerical Methods in Fluids*, Vol. 19, No. 9, 1994, pp. 765–794.

[4]Guilmineau, E., Piquet, J., and Queutey, P., "Two-Dimensional Turbulent Viscous Flow Simulation Past Airfoils at Fixed Incidence," *Computers and Fluids*, Vol. 26, No. 2, 1997, pp. 135–162

[5]Baldwin, B. S., and Barth, T. J., "A One-Equation Turbulence Transport Model for High Reynolds Number Wall-Bounded Flows," AIAA Paper 91-0610, Jan. 1991.

[6]Menter, F. R., "Zonal Two-Equation $K-\omega$ Turbulence Models for Aerodynamic Flows," AIAA Paper 93-2906, July 1993.

[7]Raffel, M., Kompenhans, J., and Wernert, P., "Investigation of the Unsteady Flow Velocity Field Above an Airfoil Pitching Under Deep Dynamic Stall Conditions," *Experiments in Fluids*, Vol. 19, 1995, pp. 103–111.

[8]McAlister, K. W., Pucci, S. L., McCroskey, W. J., and Carr, L. W., "An Experimental Study of Dynamic Stall on Advanced Airfoil Sections, Pressure and Force Data," NASA TM-84245, Dec. 1982.

[9]Carr, L. W., McAlister, K. W., and McCroskey, W. J., "Analysis of the Development of Dynamic Stall Based on Oscillating Airfoil Experiments," NASA TN-D-8382, Jan. 1977.

[10]Tuncer, I. H., Wu, J. C., and Wang, C. M., "Theorical and Numerical Studies of Oscillating Airfoils," *AIAA Journal*, Vol. 28, No. 9, 1990, pp. 1615–1624.

A. Plotkin
Associate Editor

Flowfield Measurements over an Airfoil During Natural Low-Frequency Oscillations near Stall

A. P. Broeren* and M. B. Bragg†
University of Illinois at Urbana–Champaign, Urbana, Illinois 61801

Introduction

THERE exists for flows past certain airfoils, near the onset of stall, a naturally occurring unsteady flow oscillation that is very low in frequency, with the Strouhal number typically on the order of 0.02. Here the Strouhal number is defined as $Sr = f c \sin \alpha / U_\infty$, where f is the oscillation frequency, c is the airfoil chord, α is the angle of attack, and U_∞ is the freestream speed. This low-frequency flow oscillation was studied in detail at low Reynolds numbers for an LRN(1)-1007 airfoil by Zaman et al.,[1] who concluded that the flow oscillation involved quasiperiodic switching between stalled and unstalled states. Evidence gathered from oil-flow and laser-sheet-flow visualization led Bragg et al.[2] to suggest that the unsteady stall was related to the growth and bursting of a laminar separation bubble. The oil-flow visualization also showed that the flowfield leading up to stall was two dimensional.[3]

Received May 27, 1998; revision received Sept. 19, 1998; accepted for publication Sept. 23, 1998.

*Graduate Research Assistant, Department of Mechanical and Industrial Engineering, 140 Mechanical Engineering Building, 1206 W. Green Street. Member AIAA.

†Professor, Department of Aeronautical and Astronautical Engineering, 306 Talbot Laboratory, 104 S. Wright Street. Associate Fellow AIAA.

Similar low-frequency unsteady stalling phenomena have been observed on several airfoils over a large range of Reynolds numbers.[4–6] Although much research has been carried out, the details of the unsteady flowfield and the dynamics of the laminar separation bubble remain unclear. In an effort to resolve these questions, conditionally averaged laser Doppler velocimeter (LDV) measurements were performed for the upper surface flowfield of the LRN(1)-1007 airfoil. The results of the present measurements quantified the changing character of the flowfield as the cycle of a leading-edge bubble formation, growth, merger with a growing trailing-edge separation, and resulting airfoil stall, which completes one period of the oscillation. The purpose of this Note is to present these results.

Experimental Method

All of the measurements were performed in the low-speed, low-turbulence wind tunnel at the University of Illinois. The tunnel is an open-return type, and the nominal test section dimensions are $2.8 \times 4 \times 8$ ft long. A 1-ft chord $\times$ 2.8-ft span LRN(1)-1007 airfoil model, oriented vertically in the test section and rigidly supported at each end, was used in the experiment with $\alpha = 15$ deg, $U_\infty = 50$ ft/s, and $Re = 3 \times 10^5$. At these conditions the Strouhal number was 0.021, with the dimensional frequency equal to 4.13 Hz. The angle of attack ($\alpha = 15$ deg) is approximately 2 deg below static stall, and the low-frequency oscillation has been measured as much as 3.5 deg below static stall.[3] Two components of velocity were measured at 687 locations in a single plane at the model midspan, above the airfoil upper surface and extending into the wake, as shown in Fig. 1. The measurement grid (Fig. 1) was fine enough to resolve the separation bubble approximately, yet large enough to resolve the global flowfield above the airfoil surface. The measurement location nearest the surface was at 0.005 in., or $y/c = 0.0004$ above the wall. The flow was seeded with atomized olive oil, which had a mean particle diameter of 0.6 μm (for a typical distribution, see Ref. 7). A simple first-order analysis of a seed particle's response to a step change in velocity showed that the particles were capable of adequately following the fluctuations in the unsteady, separated, and reverse flow.

The conditional-averaging method was performed with synchronization information from a hot-film sensor positioned in the airfoil wake (Fig. 1). The hot-film voltage signal shows the quasiperiodic velocity defects, characteristic of the airfoil wake that periodically engulfs the sensor. The time record of LDV data contained this information supplied from a computer program in the form of a digital-timing pulse input directly to the LDV processor master interface. The actual conditional averaging was performed during postprocessing, where several conditions were applied to each cycle as part of a validation process. Each valid cycle was divided into 24 slots in time, and the velocity data from each cycle were sorted into one of these 24 slots using a technique similar to that of Lepicovsky.[8] The result of this procedure approached a true phase-averaged representation of the flow if the oscillation was periodic. However, because the oscillation occurred naturally and the period of each cycle was not exact, there was some smearing in the conditionally averaged result. References 9 and 10 provide more details of this procedure.

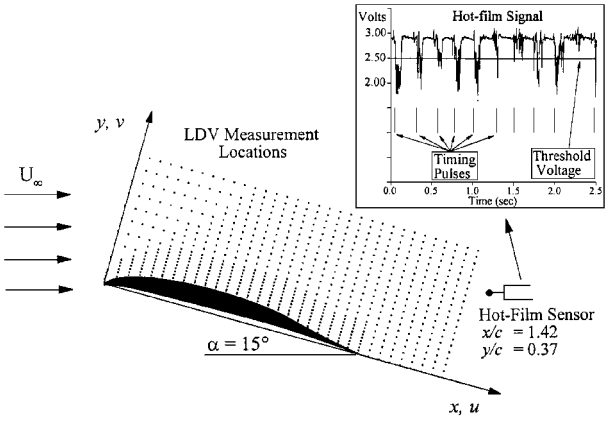

Fig. 1 Model coordinate system, hot-film sensor, and LDV measurement locations; inset: sample hot-film signal showing timing pulses.

Results

The result of the conditional-averaging method was a quantitative representation of the flowfield above the airfoil upper surface resolved over one cycle of the unsteady oscillation. The 24 time slots within a cycle resolved the oscillation into 15-deg intervals. The beginning of the cycle ($\chi = 0$ deg) was arbitrarily chosen to coincide with the timing pulses shown in Fig. 1. The velocity contours for each of the 24 time slots were plotted and analyzed to determine the behavior of the flowfield. Sample velocity contours are shown in Fig. 2. The $\chi = 30$ deg contour shows the flowfield in a separated state. The boundary layer separated at $x/c \approx 0.20$, and there was a large region of reverse flow above the airfoil's upper surface to the trailing edge and extending out into the wake. The remaining contours in Fig. 2 show a much different picture. A leading-edge separation bubble developed with a trailing-edge separation farther downstream. The locations of separation and reattachment are highlighted by the white contour line representing zero chordwise velocity. Unfortunately, the gray-scale representation of the contours does not reveal these details clearly. The color version of these plots (see Ref. 10) shows the sequence of events much more clearly.

The $\chi = 195$, 225, and 255 deg contours in Fig. 2 illustrate the growth of the leading-edge separation bubble, which is a key feature of the unsteady flowfield. The bubble initially forms at $\chi = 165$ deg (contour not shown) and is still small at $\chi = 195$ deg, and the trailing-edge separation is at $x/c \approx 0.85$. In the $\chi = 225$ deg contour, the bubble has grown in size, whereas the trailing-edge separation is located at its farthest downstream extent ($x/c \approx 0.90$). At this point in the oscillation, the trailing-edge separation begins to move forward, and the bubble continues to grow. The impending coalescence of the separation bubble reattachment and the trailing-edge separation is illustrated in the $\chi = 255$ deg contour of Fig. 2. These data show

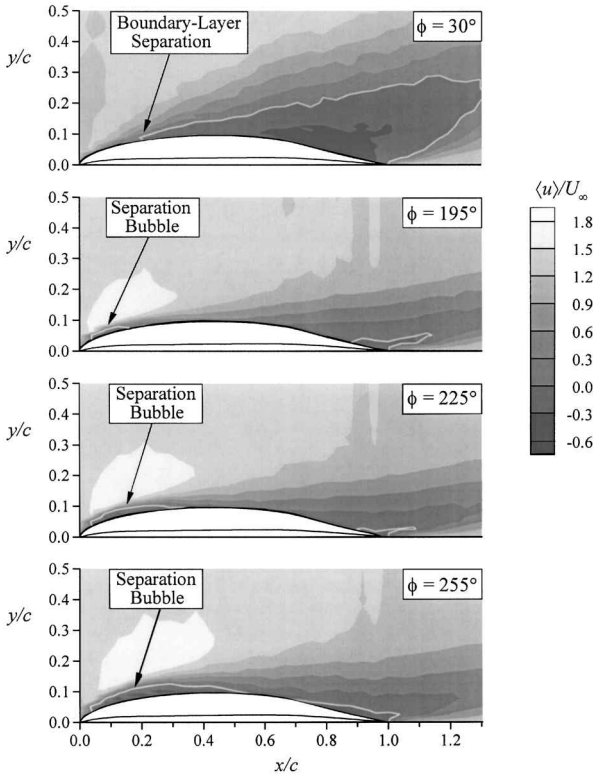

Fig. 2 Conditionally averaged chordwise velocity contours for $\phi = 30$, 195, 225, and 255 deg; the white line represents the zero velocity contour, thus delineating forward and reverse flow ($\langle u \rangle/U_\infty \pm 5\%$ and $x/c, y/c \pm 0.0002$).

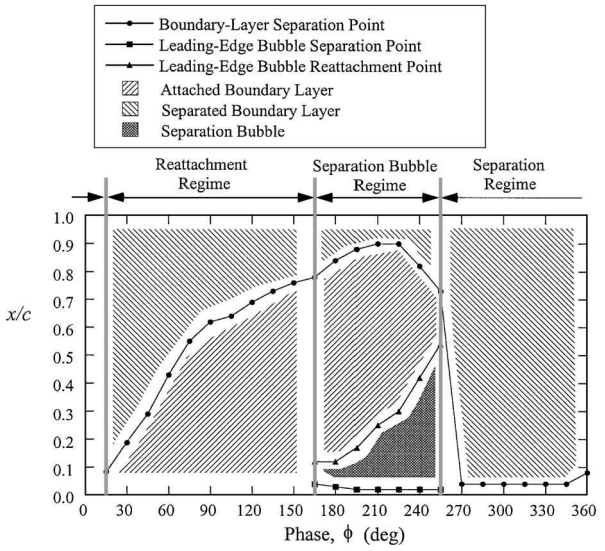

Fig. 3 Variation in the upper surface flowfield as a function of phase over the conditionally averaged cycle ($x/c \pm 0.02$).

that a separation bubble does indeed play a role in the stalling and unstalling process as previously suggested from flow visualization results.[1,2]

Further analyses of the data show that the oscillation can be divided into three distinct regimes based on the specific features that dominate the flowfield. These are illustrated in the time-dependent surface flowfield map shown in Fig. 3. The mapping shows the boundary-layer state over the conditionally averaged oscillation period. The separation and reattachment locations were obtained from the velocity profiles by extrapolating them to the wall, which provides an adequate estimate of the actual locations. In the reattachment regime, the boundary layer reattaches following the massive separation that occurred before $\chi = 15$ deg. As shown in Fig. 3, at $\chi = 15$ deg, the boundary-layer separation location is close to the leading edge and progresses downstream to about $x/c = 0.80$ at $\chi = 165$ deg. The second regime is called the separation bubble regime because the growth of the leading-edge bubble dominates the flowfield over this portion of the cycle. Figure 3 shows how the bubble grows in size during this regime. That is, the bubble separation point moves slightly forward on the airfoil as the reattachment point moves downstream with phase. As stated earlier, the boundary-layer separation point continues to move downstream until $\chi = 225$ deg and then reverses direction, moving upstream and ultimately merging with the separation bubble reattachment. Whence this occurs, the entire upper surface boundary layer is separated aft of $x/c \approx 0.05$. The coalescence of the separation bubble reattachment and the trailing-edge separation produces a large region of separated flow on the upper surface from $\chi = 255$ to 360 deg. In this separation regime, the boundary-layer separation point remains fixed at $x/c \approx 0.05$. As the boundary-layer separation point begins to move downstream, the oscillation begins again.

Conclusions

The conditionally averaged LDV data clearly show that the periodic stalling and unstalling behavior involves a leading-edge separation bubble. The data show how the bubble interacts with the trailing-edge separation in perpetuating the low-frequency oscillation.

Acknowledgments

This work was supported in part by the NASA Lewis Research Center under Grant NAG 3-1374 and also through a fellowship granted by the NASA Graduate Student Researchers Program. K. B. M. Q. Zaman of the NASA Lewis Research Center is gratefully acknowledged for his many contributions to this ongoing research.

References

[1]Zaman, K. B. M. Q., McKinzie, D. J., and Rumsey, C. L., "A Natural Low-Frequency Oscillation over Airfoils near Stalling Conditions," *Journal of Fluid Mechanics*, Vol. 202, 1989, pp. 403–442.

[2]Bragg, M. B., Heinrich, D. C., Balow, F. A., and Zaman, K. B. M. Q., "Flow Oscillation over an Airfoil near Stall," *AIAA Journal*, Vol. 34, No. 1, 1996, pp. 199–201.

[3]Heinrich, D. C., "An Experimental Study of a Low-Reynolds Number Airfoil near Stall," M.S. Thesis, Dept. of Aeronautical and Astronautical Engineering, Univ. of Illinois, Urbana, IL, 1994.

[4]Farren, W. S., "The Reaction on a Wing Whose Angle of Incidence is Changing Rapidly—Wind-Tunnel Experiments with a Short-Period Recording Balance," Aeronautical Research Council, ARC R&M 1648, His Majesty's Stationery Office, London, Jan. 1935.

[5]Bragg, M. B., Khodadoust, A., and Spring, S. A., "Measurements in a Leading-Edge Separation Bubble Due to a Simulated Airfoil Ice Accretion," *AIAA Journal*, Vol. 30, No. 6, 1992, pp. 1462–1467.

[6]Mabey, D. G., "Review of Normal Force Fluctuations on Aerofoils with Separated Flow," *Progress in Aerospace Sciences*, Vol. 29, No. 1, 1992, pp. 43–80.

[7]"Model 9306 6-Jet Atomizer Instruction Manual," TSI, Inc., St. Paul, MN, June 1987.

[8]Lepicovsky, J., "Laser Velocimeter Measurements of Large-Scale Structures in a Tone-Excited Jet," *AIAA Journal*, Vol. 24, No. 1, 1986, pp. 27–31.

[9]Broeren, A. P., and Bragg, M. B., "Phase-Averaged LDV Flowfield Measurements About an Airfoil in Unsteady Stall," *Proceedings of the AIAA 14th Applied Aerodynamics Conference*, AIAA, Reston, VA, 1996, pp. 921–931 (AIAA Paper 96-2494).

[10]Broeren, A. P., "Phase-Averaged Flowfield Measurements About an Airfoil in Unsteady Stall," M.S. Thesis, Dept. of Mechanical and Industrial Engineering, Univ. of Illinois, Urbana, IL, 1996.

M. Samimy
Associate Editor

Extracting Second-Order Systems from State-Space Representations

M. I. Friswell*
University of Wales Swansea, Swansea, Wales SA2 8PP, United Kingdom
S. D. Garvey† and J. E. T. Penny‡
Aston University, Birmingham, England B4 7ET, United Kingdom

I. Introduction

IT is established that every linear dynamic system that can be modeled using a finite number of degrees of freedom can be cast in state-space form. The so-called modern control literature has adopted this form almost globally and to good effect. Systems of second-order differential equations are transformed into first-order (state-space) form at the instant that the characteristic roots are required or when any active control is envisaged. Occasionally, however, the reverse transformation is useful. In modal testing, system realization methods such as the eigensystem realization algorithm[1] produce an input–output representation of the measured data, which is essentially a state-space model. Other applications include the reduction of highly damped structural models and the electromagnetic dynamics of large electrical machines.

It would appear that little attention has been given in the literature to this transformation. Alvin and Park[2] and Alvin et al.[3] considered the transformation from state-space to second-order form.

Received May 2, 1998; revision received Oct. 3, 1998; accepted for publication Oct. 5, 1998.

*Reader, Department of Mechanical Engineering.
†Reader, School of Engineering.
‡Senior Lecturer, School of Engineering.